

PCCP

Accepted Manuscript



This is an *Accepted Manuscript*, which has been through the Royal Society of Chemistry peer review process and has been accepted for publication.

Accepted Manuscripts are published online shortly after acceptance, before technical editing, formatting and proof reading. Using this free service, authors can make their results available to the community, in citable form, before we publish the edited article. We will replace this *Accepted Manuscript* with the edited and formatted *Advance Article* as soon as it is available.

You can find more information about *Accepted Manuscripts* in the [Information for Authors](#).

Please note that technical editing may introduce minor changes to the text and/or graphics, which may alter content. The journal's standard [Terms & Conditions](#) and the [Ethical guidelines](#) still apply. In no event shall the Royal Society of Chemistry be held responsible for any errors or omissions in this *Accepted Manuscript* or any consequences arising from the use of any information it contains.

Adsorption of Guanidinium Collectors on Aluminosilicate Mineral—A Density Functional Study

Nulakani Naga Venkateswara Rao ^a, Prathab Baskar^b, Abhay Shankar Patra^b and Venkatesan Subramanian^{a*}

^aChemical Laboratory, CSIR-Central Leather Research Institute, Adyar, Chennai - 600 020, India.

^bResearch & Development, Tata Steel Limited, Jamshedpur 831 001, India.

Abstract

In this density functional theory based investigation, we have modelled and studied the adsorption behaviour of guanidinium cation and substituted (phenyl, methoxy phenyl, nitro phenyl and di-nitro phenyl) guanidinium cationic collectors on the basal surfaces of kaolinite and goethite. The adsorption behaviour is assessed in three different media, such as gas, explicit water and pH medium to understand the affinity of GC collectors with the SiO₄ tetrahedral and AlO₆ octahedral surfaces of kaolinite. The tetrahedral siloxane surface possesses larger binding affinity with GC collectors than the octahedral sites due to the presence of surface exposed oxygen atoms that are active in the intermolecular interactions. Further, the inductive electronic effects of substituted guanidinium cations also play a key role on the adsorption mechanism. Highly positive cations result in a stronger electrostatic interaction and preferential adsorption with the kaolinite surfaces than low positive cations. Computed interaction energies and electron densities at the bond critical points suggest that the adsorption of guanidinium cations on the surfaces of kaolinite and goethite is due to the formation of intra/inter hydrogen bonding networks. Also, the electrostatic interaction favours the high adsorption ability of GC collectors in the pH medium than gas phase and water media. The structures and energies of GC collectors pave an intuitive view for future experimental studies on mineral flotation.

Corresponding Author

*E-mail: subbuchem@hotmail.com; subbu@clri.res.in;

Tel.: +91 44 24411630. Fax: +91 44 24911589

1 Introduction

In the last two decades the applications of electronic structure methods to various challenging problems have increased several folds due to significant advancements in computer hardware and development of highly reliable methodologies. Particularly, employment of density functional theory (DFT) in various fields to unravel important questions increases steadily.¹ The DFT methods have been applied to unravel structure and reactivity,² spectra of molecules³ including absorption and emission spectra, interaction of protein (DNA)-ligand interactions⁴⁻⁶ including drug-discovery⁷ and also to gain insight into different questions in materials science.⁸⁻¹⁰ Parenthetically, another promising new field of application of DFT methods is unravelling the flotation process of minerals. In flotation, chemical species adsorb onto mineral/water interfaces in order to control their hydrophilic/hydrophobic character.¹¹ The capacity of a mineral to adsorb selectively a particular reagent molecule depends on a wide range of chemical, thermodynamic and steric factors. For the beneficiation of multicomponent, highly disseminated and difficult to-treat ore deposits, the conventional approaches of reagent design and selection are inadequate. A quantitative methodology to screen out/identify the appropriate molecular architectures from theoretical computations, is evidently an economically attractive and elegant methodology as compared to the experimental approach.¹² Selecting the most prominent molecule based on computational chemistry approaches for subsequent synthesis, characterisation and pilot plant/plant trials will certainly save enormous costs in time and efforts to arrive at new formulations.¹³

For mineral flotation systems, there are a number of reagents available in the form of collectors, frothers, modifiers, depressants, dispersants, etc., that are used to enhance the adsorption process so that valuable mineral particles can be separated from the gangue particles.¹⁴ In flotation practice, the collector consists of a functional group that is polar and a

nonpolar hydrocarbon chain or a polymeric compound. The selectivity of the collector and mineral interaction is determined by the characteristic of the functional group and the nature of the hydrocarbon chain. Froth flotation of iron ore is a well-established industrial practice. Goethite was identified as the major iron bearing mineral phase and kaolin as gangue phase in the slime.¹⁵ Iron ore minerals like goethite can be floated by a variety of collectors, such as amines, oleates, sulfonates and sulfates.^{16,17} Beneficiation of iron ore slimes containing significant amount of Fe along with SiO₂ and Al₂O₃ can be concentrated either by reverse cationic flotation of aluminosilicates (kaolin) or direct anionic flotation of Fe. The cationic reverse flotation of aluminosilicates seems to be an attractive route for the concentration of low grade ores.¹⁸ In this work, adsorption studies on iron ore will be investigated using guanidine based cationic collectors. Zhao,¹⁹ Hu²⁰ and Wang²¹ have extensively investigated the flotation mechanism of kaolinite using different types of amines including alkylamines, ether-amines and quaternary ammonium salts. They found that flotation mechanisms are mainly controlled by the electrostatic effect, hydrogen-bonding and solution chemistry. Design and selection of novel cationic flotation reagents tailor-made for reverse flotation is a challenging task. In this connection, we have examined various possible candidates. Amongst, guanidine is one of the strongest bases (pKa =13.6) with strong hydrogen bonding capability and chemical stability which has all possible parameters for cationic collector.²² Furthermore, limited information is available on the applications of guanidine in the reverse flotation of iron ore slime. Hence, guanidine has been chosen for the present investigation as a collector to model floatation process. Various derivatives of guanidine considered in this investigation are guanidinium cation (GC), phenyl guanidinium cation (PGC), p-methoxy phenyl guanidinium cation (MPGC), p-nitro phenyl guanidinium cation (NPGC) and 3, 5-dinitrophenyl guanidinium cation (DNPGC). With the help of above-mentioned derivatives,

the effect of substitution of $-\text{C}_6\text{H}_5$, $-\text{C}_7\text{H}_7\text{O}$, $-\text{C}_6\text{H}_4\text{NO}_2$ and $-\text{C}_6\text{H}_3(\text{NO}_2)_2$ groups have been studied and their role in the flotation of kaolinite has also been assessed.

The objective of this work is to unravel the adsorption behaviour and mechanism of a series of guanidinium cations on kaolinite as well as the influence of the substituent effect on the performance of guanidinium cations in floatation. Further, adsorption of same guanidine and its derivatives has also been studied on the goethite mineral to predict the trend in the selectivity of guanidine based collectors.

2 Methods and models

2.1 Quantum chemical methods

All calculations were carried out within the framework of Density Functional Theory (DFT) using the B3LYP functional as implemented Gaussian 09 suit of program.²³ The 6-31G(d) basis set was used for the elements H, C, N, O, Al and Si atoms whereas the effective core potential basis set such as LANL2DZ was used for the Fe atoms in the geometry optimization. The cationic collectors, the inorganic mineral surfaces and their complexes were fully optimized without any geometrical constrains in gas, solvent and pH medium. The binding energy (BE) of the collectors on the mineral surfaces in three different media was calculated using the following formula

$$BE = E_{\text{Complex}} - (E_{\text{Collector}} + E_{\text{surface}})$$

The BEs were calculated by employing the B3LYP functional and 6-31G (d), 6-31G (d,p) and 6-31G+(d,p) basis sets using the geometries optimized at B3LYP/6-31G(d) level of theory. These binding energies were corrected for basis set superposition error (BSSE) using counterpoise (CP) procedure suggested by Boys and Bernardi.²⁴ The AIM methodology²⁵ was used to analyse the electron density $\rho(r_c)$ and its Laplacian ($\nabla^2\rho(r_c)$) at the hydrogen bond critical points (HBCPs). The wave functions calculated from the B3LYP/6-31G (d) level of theory were used to generate AIM molecular graphs for all the complexes. In general, a large

total electron density $\rho(r_c)$ at the BCPs of collector and surface indicates the presence of HB and the positive value of Laplacian of Electron Density ($\nabla^2\rho(r_c)$) at the bond critical points implies the closed-shell (electrostatic) nature of interaction. The solvent effect (water) was modelled by adding water molecules explicitly in the proximity of interacting region of the collector and mineral surface. Further, the polarizable continuum model²⁶ (PCM) self-consistent reaction field was also adopted on the top of explicit water model to analyse the trend in the binding energies. To model the pH medium with in the frame work of DFT, the hydrogen atoms at the surface of the inorganic minerals were deprotonated similar to the previous studies^{27,28}. This creates a pH regime which is above the zero-point charge of respective mineral surface.

2.2 Models of Collectors and Minerals

Guanidinium based cationic collectors such as guanidinium cation (GC), phenyl guanidinium cation (PGC), p-methoxy phenyl guanidinium cation (MPGC), p-nitro phenyl guanidinium cation (NPGC) and 3, 5-dinitrophenyl guanidinium cation (DNPGC) as well as the inorganic mineral surfaces such as kaolinite and goethite clusters were taken for modelling. The optimized geometry of GC is shown in Fig. 1a. The GC contains a unit positive charge with the molecular formula $[C(NH_2)_3]^+$ and belongs to the D_3 point group.²⁹ It has three $-NH_2$ groups which are trigonally projected outward from the central carbon atom. The three $-NH_2$ groups are tilted at an angle of $\sim 14.5^\circ$ from the planar structure. All the C–N bond distances are equal to 1.34 Å and the C–N–C bond angle is close to 120° . The optimized geometries of other substituted guanidinium collectors such as PGC, MPGC, NPGC and DNPGC are also depicted in Fig. 1.

The inorganic cluster models were constructed from the experimental periodic structure as shown in the Fig. 2. Kaolinite is a layered aluminosilicate in which each layer is composed of a sub-layer of corner sharing SiO_4 tetrahedra and a sub-layer of edge sharing AlO_6 octahedra.

The individual layers are held together due to the presence of hydrogen bonding between the hydroxyl groups of AlO_6 octahedra and siloxane of SiO_4 tetrahedra.^{30,31} From this experimental periodic structure, a neutral kaolinite cluster (see Fig. 2a) with the molecular formula $\text{Al}_6\text{Si}_6\text{O}_{36}\text{H}_{30}$ were constructed similar to those used in several previous studies^{32,33}. It has two basal surfaces as shown in Fig. 2b, c. The AlO_6 octahedral surface is denoted as K(a) surface (shown in Fig. 2b) and the SiO_4 surface is referred to as K(s) surface (shown in Fig. 2c) in the remaining part of the text. In addition, iron oxide cluster with two FeO octahedrons³⁴ as a model for the goethite phase with the molecular formula $\text{Fe}_2\text{O}_3(\text{H}_2\text{O})_7$ was also considered (see Fig. 2d). The previous studies³²⁻³⁴ utilizing cluster models for mineral surfaces emphasized the reliability of cluster approach for adsorption studies.

3 Results and discussions

3.1 Adsorption of GC on kaolinite and goethite

The optimized geometries of GC on the basal surfaces of kaolinite and goethite clusters are depicted in Fig. 3, along with hydrogen bonds (HBs). Based upon the strength of binding energy, the HBs are classified into three types such as strong ($E_{\text{HB}} = > 15$ kcal/mol), moderate ($E_{\text{HB}} = 4$ to 15 kcal/mol) and weak ($E_{\text{HB}} < 4$ kcal/mol). Mostly, the strong HBs are normally coupled with the shorter HB lengths with the HB angle $\angle (\text{D}-\text{H}\cdots\text{A})$ close to 180° , while the weaker HBs are generally longer with the HB angle close to 90° .

The binding energies of GC on kaolinite were calculated for two initial conformations such as parallel and perpendicular with respect to the planes of K(a) as well as K(s) surfaces. The optimized geometries of GC on the basal surfaces of kaolinite and goethite clusters are depicted in Fig. 3. The GC was placed parallel to K(a) surface and it was fully relaxed (equilibrium conformation). In the equilibrium geometry, the parallel conformation of GC turned to perpendicular conformation as shown in Fig. 3a. Close analysis on the geometry of GC-K(a) complex reveals that the adsorption is mainly determined by the hydrogen bonding

interaction between the one $-\text{NH}_2$ group of GC with the two oxygen atoms of K(a) surface. The hydrogen bonding interactions are represented using black dashed lines in all the complexes. The other two $-\text{NH}_2$ groups point away from the mineral surface. The calculated binding energies of guanidinium based collectors with the three inorganic mineral surfaces using three different basis sets are listed in Table 1. The calculated binding energies using 6-31G(d) and higher basis set 6-31G(d,p) show nearly the same interaction energy for all the collector-mineral complexes whereas 6-31G+(d,p) yields marginally less binding energy. Further, there is no substantial change in the relative trend of the binding energies of all the complexes with higher basis set calculations. Hence, the binding energy calculations with 6-31G (d) basis set are considered for the further study. The binding energy of GC on K(a) surface with two HB formation is -27.57 kcal/mol. These two HBs are represented as HB1 ($-\text{NH}\cdots\text{O} = 1.77 \text{ \AA}$, $\angle\text{NH}\cdots\text{O} = 151.38^\circ$) and HB2 ($-\text{NH}\cdots\text{O} = 1.90$, $\angle\text{NH}\cdots\text{O} = 142.33$). The calculated HB parameters of all the collector-mineral complexes are listed in Table 2. It indicates that HB1 is a stronger hydrogen bond when compared to HB2. The corresponding $\rho(r_c)$ values of HB1 (0.0402 a.u) and HB2 (0.0302 a.u) which further substantiates that HB1 is stronger than HB2. Calculated AIM molecular graphs for the various cation-mineral complexes are given in Supporting Information (Fig. S1-S3).

Unlike K(a) surface, the K(s) surface is free from surface hydrogen atoms. Even though GC is placed parallel to the K(s) surface, the optimization leads to an inclined conformation with an inclination of 45° to K(s) surface as depicted in Fig. 3b. The GC forms three HBs through two $-\text{NH}_2$ groups and the third $-\text{NH}_2$ group is away from the K(s) surface. The first $-\text{NH}_2$ group forms two HBs such as HB1 ($-\text{NH}\cdots\text{O} = 1.93$, 173.85) and HB2 ($-\text{NH}\cdots\text{O} = 2.43$, $\angle\text{NH}\cdots\text{O} = 146.46$). The second $-\text{NH}_2$ group forms only one HB, HB3 ($-\text{NH}\cdots\text{O} = 1.93$, $\angle\text{NH}\cdots\text{O} = 159.14$) with O atoms of SiO_4 tetrahedron. The calculated $\rho(r_c)$ values for HB1, HB2 and HB3 are 0.0277, 0.0096 and 0.0284 a.u, respectively. These values

point out that the HBs of GC on K(s) surface are individually weaker than that of K(a) in accordance with the longer $\text{-NH}\cdots\text{O}$ HB distance and marginal electron density values. However, the resulting binding energy of GC on K(s) surface is twofold higher (-43.51 kcal/mol) than that of GC on K(a) surface due to the formation of three HBs and additional electrostatic interaction between the two systems. All these interactions lead to the formation of GC-K(s) complex with binding energy of -43.51 kcal/mol. The goethite cluster is investigated to determine the preferential adsorption tendency of guanidine over kaolinite surfaces. Similar to the kaolinite surfaces, the GC is stabilized by hydrogen bonding interactions with the goethite cluster. The GC perpendicularly interacts with the goethite cluster as presented in Fig. 3c. Two -NH_2 groups of GC are responsible for the formation of two hydrogen bonds (HB1 ($\text{-NH}\cdots\text{O} = 1.61$, $\angle\text{NH}\cdots\text{O} = 176.43$) and HB2 ($\text{-NH}\cdots\text{O} = 1.79$, $\angle\text{NH}\cdots\text{O} = 176.07$)) with the oxygen atoms of the goethite cluster. The $\rho(r_c)$ of HB1 and HB2 is 0.0588 and 0.0385 a.u which reveals that stronger HBs are formed between GC and goethite. Although other mode of interaction of GC with goethite cluster has been investigated, they exhibit relatively less binding energy than the perpendicular conformation. The hydrogen bonding interactions of GC with goethite cluster lead to the formation complex with binding energy of -40.10 kcal/mol. Overall, the binding energy of GC with three different mineral surfaces is as follows, $\text{GC-K(s)} < \text{GC-Goethite} < \text{GC-K(a)}$. This trend elicits that GC preferentially adsorbs on K(s) surface of kaolinite over goethite mineral.

3.2 Adsorption of PGC, MPGC, NPGC and DNP GC on kaolinite and goethite

To elucidate the substituent effect on the adsorption capacity of GC, the aromatic guanidinium cations substituted with electron donating and withdrawing groups have been chosen. The optimized geometries of substituted guanidinium cationic collectors on K(a) surface are depicted in Fig. 4. The addition of phenyl ring to the GC reduces the binding strength of GC on the K(a) surface (see Table 1). The PGC forms two hydrogen bonds HB1

($-\text{NH}\cdots\text{O} = 1.83$, $\angle\text{NH}\cdots\text{O} = 146.91$) and HB2 ($-\text{NH}\cdots\text{O} = 1.91$, $\angle\text{NH}\cdots\text{O} = 144.44$) which are akin to GC (as shown in Fig. 4b). The corresponding $\rho(r_c)$ value at the bond critical points of HB1 and HB2 is 0.0355 and 0.0305 a.u. The low total electron densities at the bond critical points (i.e., low $\rho(r_c)$ values) and longer HB lengths of PGC on K(a) surface indicate that, these HBs are weaker than that of GC. Hence, PGC exhibits less binding energy of -23.94 kcal/mol than GC (-27.57 kcal/mol). The introduction of methoxy (-OCH₃) group at the para position of the PGC (i.e., MPGC) further decreases the binding energy (-22.71 kcal/mol). The MPGC forms two HBs with the O atoms of K(a) surface similar to that of GC and PGC (see Fig. 4c). It is evident from Table 2 that, the hydrogen bonding parameters of PGC and MPGC on K(a) surface are similar to those of GC. However, the binding energy of PGC and MPGC is less than that of GC. This may be due to decrease in electrostatic interaction in the collector-mineral complex owing to delocalization of positive charge of guanidinium over the phenyl ring in PGC and MPGC. Further, the MPGC contains an extra electron donating (methoxy) group on the phenyl ring which makes the MPGC further electron rich. The unit positive charge on guanidine unit and higher electron density on phenyl ring of MPGC balances each other and results in net decrease in the cationic charge. It is realised that the incorporation of electron withdrawing groups on phenyl ring will increase the binding strength. The NPGC has binding energy (-27.13 kcal/mol) which is closer to that of GC on the K(a) surface. It forms two HBs exhibiting a shorter HB lengths and higher bond angles (HB1 ($-\text{NH}\cdots\text{O} = 1.88$, $\angle\text{NH}\cdots\text{O} = 144.75$) and HB2 ($-\text{NH}\cdots\text{O} = 1.80$, $\angle\text{NH}\cdots\text{O} = 148.32$)) than those of PGC and MPGC. The increased $\rho(r_c)$ at the HB critical points and decreased bond lengths reveal that, the HBs formed by NPGC are stronger than that of PGC and MPGC. Further, these HBs are similar to those of GC. A stronger electron withdrawing ability of -NO₂ results in a larger net positive charge on guanidine unit. It increases the hydrogen bonding and electrostatic interactions of NPGC with K(a) surface. The introduction

of second $-\text{NO}_2$ group further increases the binding energy and as a result adsorption capacity. The higher binding energy of DNPGC with K(a) surface is due to increased electrostatic interactions and the formation of additional HBs between $-\text{NO}_2$ group of cation and hydroxyl groups of K(a) surface. The DNPGC forms two HBs through guanidine and two HBs with the aid of one of its $-\text{NO}_2$ group as shown in Fig. 4d. Two $-\text{NH}_2$ groups of guanidine facilitate two HBs such as HB1 ($-\text{NH}\cdots\text{O} = 1.77$, $\angle\text{NH}\cdots\text{O} = 156.71$) and HB2 ($-\text{NH}\cdots\text{O} = 1.73$, $\angle\text{NH}\cdots\text{O} = 166.91$) with the oxygen atoms of K(a) surface. Further, one $-\text{NO}_2$ group of DNPGC forms two HBs such as HB3 ($-\text{NO}\cdots\text{H} = 2.39$, $\angle\text{NO}\cdots\text{H} = 137.56$) and HB4 ($-\text{NO}\cdots\text{H} = 2.20$, $\angle\text{NO}\cdots\text{H} = 153.30$) with the hydroxyl groups of K(a) surface. The larger $\rho(r_c)$ (see Table 2) and shorter bond lengths of HB1 and HB2 point out that these are stronger than all the other HBs formed by guanidine collectors in this series. The two strong electron withdrawing groups enhance the net cationic charge on guanidinium unit in DNPGC. The stronger HBs and increased electrostatic interactions in DNPGC-K(a) complex results in the formation of complex with binding energy of -33.67 kcal/mol which is significantly higher than all other collector-K(a) complexes (see Table 1). Overall the binding energies of five different guanidinium based cationic collectors on K(a) surface are found to be $\text{MPGC} > \text{PGC} > \text{GC} \sim \text{NPGC} > \text{DNPGC}$.

On the other hand, the four substituted guanidinium cationic collectors such as PGC, MPGC, NPGC and DNPGC exhibit similar conformation to that of GC on both K(s) surface (see Fig. 5) and goethite cluster (see Fig. 6). The calculated binding energies are listed in Table 1 and HB parameters for all the collectors on different surfaces are summarized in Table 2. It is evident from the Table 1 and Fig. 7a that, the guanidinium based cationic collectors have comparatively higher adsorption capacity on K(s) surface than on K(a) surface and goethite cluster. The higher adsorption of cationic collectors on K(s) surface is governed by the formation of additional hydrogen bond (HB3) and increased electrostatic

interactions between collector-K(s) complexes. In gas phase, for a particular collector the binding energies on three different surfaces vary as $K(s) < \text{Goethite} < K(a)$, while on a particular surface the trend in binding energies of five different collectors is found to be $\text{MPGC} > \text{PGC} > \text{GC} \sim \text{NPGC} > \text{DNPGC}$. These results are in consistent with the previous theoretical and experimental studies,³⁵⁻³⁷ which states that the cationic collectors show the stronger interaction energy with the K(s) surface than that of K(a) surface. The binding energies of various cationic collectors calculated using 6-31G(d,p) and 6-31+G(d,p) basis sets were also show the same trend (see Fig.S4).

3.3 Effect of solvation

All the calculations were carried in water environment to compare the results with those obtained from experimental conditions. An explicit water model with four water molecules and an implicit water model on the top of the explicit water model were chosen to describe discrete solvation effect on the interaction of collector with mineral surfaces. In explicit water model, four water molecules were added to the collector-mineral complexes nearer to the interacting region and the geometry of the complexes were minimized. The added water molecules form intra/intermolecular hydrogen bonding networks with the mineral surfaces.

The calculated HB parameters of all guanidinium based cationic collectors in explicit water model are presented in Table 3. The optimized geometry of GC in the presence of four explicit water molecules is given in Fig. 8a. The presence of explicit water molecules around the interacting region of GC-K(a) complex induces slight changes in the orientation of GC when compared to that of gas phase results. Unlike the gas phase findings, the GC is stabilized at the centre of the K(a) surface. However, the GC forms two HBs such as HB1 ($-\text{NH}\cdots\text{O} = 2.18$, $\angle\text{NH}\cdots\text{O} = 121.20$) and HB2 ($-\text{NH}\cdots\text{O} = 1.98$, $\angle\text{NH}\cdots\text{O} = 147.16$) with the O atoms of K(a) surface. Further, the GC is more strongly attracted to the water molecule

through the formation of HB of the type ($-\text{NH}\cdots\text{O}_{\text{wat}}$) than to the O atoms of kaolinite. However, this interaction does not contribute to the stabilization of GC on the hydrated K(a) surface. The binding energy of GC in explicit water is around -12.02 kcal/mol which is ~ 15 kcal/mol less than that of gas phase on K(a) surface. The calculated electron densities at the HB critical points and the slightly elongated bond lengths and binding energies of GC reveal that it is less stable in explicit water than in gas phase on K(a) surface.

On the other hand, the presence of explicit water molecules orients the GC to the centre of the K(s) surface and form two moderate HBs such as HB1 ($-\text{NH}\cdots\text{O} = 2.39$, $\angle\text{NH}\cdots\text{O} = 152.23$) and HB2 ($-\text{NH}\cdots\text{O} = 2.16$, $\angle\text{NH}\cdots\text{O} = 135.55$) as depicted in Fig. 8b. Consequently, the binding energy of GC decreases by ~ 10.0 kcal/mol in explicit water than in gas phase. Similar to the K(a) and K(s) surfaces, the discrete solvation destabilizes interaction of GC with goethite. The GC forms two HBs with the goethite cluster which are described as HB1 ($-\text{NH}\cdots\text{O} = 1.77$, $\angle\text{NH}\cdots\text{O} = 172.01$) and ($-\text{NH}\cdots\text{O} = 1.96$, $\angle\text{NH}\cdots\text{O} = 166.35$). The slight changes in the GC orientation on Goethite in the presence of water molecules (see Fig. 8c) leads to marginal reduction in the binding energy (~ 9 kcal/mol) when compared to that of gas phase.

In the presence of water molecules, the substituents PGC, MPGC, NPGC and DNPGC adopt similar conformation as that of gas phase on K(a) surface. To avoid redundancy, the structures of these complexes are not presented. The binding energy of PGC, MPGC and NPGC is found to be -4.0, -7.0 and -8.0 kcal/mol, respectively. This is due to the disruption of one HB in the presence of explicit water molecules when compared to gas phase complex. However, DNPGC shows a binding energy of -14 kcal/mol in the discrete solvation model as it is anchored by $-\text{NO}_2$ group on K(a) surface through additional HBs such as HB3 and HB4 which are akin to that of gas phase.

The presence of explicit water molecules orients PGC, MPGC, NPGC and DNP GC to form HB1 and HB2 with K(s) surface similar to that of GC (see Fig. 8b). The larger $\rho(r_c)$ values of HB2 corresponds to higher binding strength of cationic collectors on K(s) compared to K(a) surface. In the case of goethite cluster, all the substituted collectors exhibit nearly the same orientation as that of GC in the presence of explicit water molecules. Overall, the addition of explicit water molecules to the collector-mineral complex decreases the binding energy of cationic collectors on the mineral surfaces. The slight changes in the collector orientation on the mineral surfaces are induced by explicit water molecules. These are responsible for the reduction in the binding energies. Although the binding energies slightly decrease in explicit water models, they follow the same trend as that observed in gas phase. On the other hand, the implicit solvation effect is also modelled on the top of optimized geometries of explicit water model by including the polarizable continuum model (PCM) self-consistent reaction field. Table 1 shows that the binding energies are considerably lower than that of gas and explicit water models. However, the binding energy trend of implicit calculations is not altered upon explicit water model is not altered and akin to those of gas phase and explicit water medium results. The low binding efficiency of cationic collectors on the K(a) surface in explicit water is completely destroyed in the implicit on explicit water model and it does not offer any favourable binding energies. Parenthetically, substituent effects of guanidinium cations and binding energies behaviour are same as that of gas or explicit water model.

3.4 Effect of pH.

The adsorption response of a mineral is dependent on the pH of the medium. The kaolinite surfaces exhibit different surface properties at different pH strengths. It is known from the definition of zero point charge (ZPC), the oxide surface exhibits a net positive charge at the pH value below its ZPC and participate in anion attraction.³⁸ While the oxide

surface exhibits a net negative charge at pH above ZPC and it attracts cationic collectors. Hence we tested the adsorption capabilities of guanidinium based cationic collectors at a pH value which is higher than the ZPC of kaolinite. Moreover, as the pH increases above ZPC, the anionic charge density increases on the mineral surfaces. The ZPC value of kaolinite is around 4.6³⁸⁻⁴⁰ and that of goethite is around 8.0³⁸ indicating that the ZPC value of goethite is nearly two fold higher than that of kaolinite. At a particular pH value which is above the ZPC of goethite, the goethite cluster carries a less net negative charge than that of kaolinite. It is found from previous reports⁴¹ that the hydroxyl groups of K(a) surface are transformed into oxy anions at pH > 8.5. Theoretically, the pH effect is modelled based on addition or removal of protons to a particular surface.^{27,28} Hence, to study the interaction between the cationic collectors and K(a) surface, four –OH groups of K(a) surface were deprotonated. Similarly, we have removed four protons of the K(s) surface which are added in the form of hydrogen atoms to maintain the electro neutrality in the cluster. At the same time, pH 8.5 is very nearer to the ZPC of goethite, it creates a less anionic charge density compared to that of kaolinite. Hence, we have removed two protons of goethite cluster. Overall, the kaolinite surface carries a net negative charge of $-4 e^-$ whereas the goethite cluster carries a net negative charge of $-2 e^-$. As a result the electrostatic interaction is drastically enhanced between the cationic collectors and negatively charged mineral surfaces. These findings agree with the previous reports on the ionization magnitude of kaolinite and adsorption with pH.⁴² The binding energies and bonding parameters of all the cationic collectors on three mineral surfaces in the pH model are listed in Tables 1 and 4, respectively. The binding energy profile of cationic collectors in the pH model is presented in Fig. 7c. The cationic collectors form extra HBs due to the presence of excess negative charge on the mineral surfaces. For K(a) surface, GC utilizes four of its hydrogen atoms and forms four HBs which are described as HB1 ($-NH\cdots O = 1.91$, $\angle NH\cdots O 142.66$), HB2 ($-NH\cdots O = 1.60$, $\angle NH\cdots O 162.54$), HB3 ($-NH\cdots O$

= 2.66, $\angle\text{NH}\cdots\text{O}$ 133.65) and HB4 ($-\text{NH}\cdots\text{O}$ = 2.09, $\angle\text{NH}\cdots\text{O}$ 145.77). The remaining two hydrogen atoms are oriented away from the mineral surface as depicted in Fig. 9a. In the case of K(s) surface, GC forms six HBs using all of its hydrogen atoms as shown in Fig. 9b. The presence of freely exposed O atoms on K(s) surface makes GC possible to form six HBs. On the other hand, the guanidinium cation transfers one of its protons to the negatively charged goethite cluster reducing the net negative charge on goethite cluster and the cationic collector becomes neutral (see Fig. 9c). This leads to the decrease in binding energies between the collector and goethite cluster.

On moving to the substituted cationic collectors (PGC, MPGC, NPGC and DNPGC), the presence of phenyl ring in these collectors slightly disturbs the actual HBs formed by GC on K(a) and K(s) surfaces. Therefore, the substituted cationic collectors form less HBs on each mineral surface due to the presence of steric repulsion between the kaolinite surface and phenyl rings. On the other hand, these collectors adopt similar geometrical orientations on goethite cluster as that of GC. All the bonding patterns of PGC, MPGC, NPGC and DNPGC on the three inorganic mineral surfaces are presented in Fig. S5. The electron donating and withdrawing effects of cationic collectors orchestrate on the binding energies in the same way as observed in gas phase and discrete solvation model. Table 1 and Fig. 7c show the influence of negative surface charge is larger in the case of adsorption of guanidinium collectors on the kaolinite surfaces than goethite cluster. Comparison of binding energies of guanidinium based cationic collectors with kaolinite and goethite surface indicates that preferential selectivity of GC based collectors is higher for kaolinite surface. Further, Zhong Hong and his research group⁴³ experimentally observed the flotation mechanism of aluminosilicate minerals using alkylguanidine collectors through flotation experiments, Zeta potential measurements and FT-IR spectrum analysis. The flotation analysis reflects the adsorption trend predicted in the the present study.

4 Conclusions

The adsorption capacities of guanidinium based cationic collectors on the kaolinite and goethite surfaces have been investigated using the DFT based calculations. The five cationic collectors such as guanidinium cation (GC), phenyl guanidinium cation (PGC), p-methoxy phenyl guanidinium cation (MPGC), p-nitro phenyl guanidinium cation (NPGC) and 3, 5-dinitrophenyl guanidinium cation (DNPGC) are selected for the present investigation. It is found from the calculation that the electron withdrawing groups enhances the adsorption capacity while the electron donating groups suppress the same. The binding of collectors on kaolinite and goethite depends mostly on its capability to form hydrogen bonds with the hydroxyl groups of the aluminum–oxygen surface or with the basal oxygen atoms of the siloxane or with oxygen atoms of goethite. The collectors exhibit higher binding energy on siloxane surface of kaolinite followed by goethite and alumina surface of kaolinite in gas phase. The same trend is observed in explicit water medium. However, the ionisation of mineral surfaces (pH medium) dominates the binding energies of collectors. Accordingly, the energy of molecular adsorption of Guanidinium collector-kaolinite mineral complex is highly negative indicating the interaction energy obtained is considered to be a quantitative measure of the intensity of collector binding efficiency and floatability with kaolinite minerals.

Acknowledgment The authors would like to thank Tata Steel Limited, Jamshedpur, India and Multi-Scale Simulation and Modeling (MSM) project (CSC0129), CSIR for providing financial support.

References

1. R. A. Friesner, *Proc. Natl. Acad. Sci.*, 2005, **102**, 6648–6653.
2. T. Ziegler and J. Autschbach, *Chem. Rev.*, 2005, **105**, 2695–2722.
3. C. W. Bauschlicher and S. R. Langhoff, *Chem. Rev.*, 1991, **91**, 701–718.
4. P. U. Maheswari, V. Rajendiran, M. Palaniandavar, R. Parthasarathi, and V. Subramanian, *J. Inorg. Biochem.*, 2006, **100**, 3–17.
5. K. Subramanian, D. Jia, P. Kapoor-Vazirani, D. R. Powell, R. E. Collins, D. Sharma, J. Peng, X. Cheng, and P. M. Vertino, *Mol. Cell*, 2008, **30**, 336–347.
6. R. Vijayalakshmi, M. Kanthimathi, V. Subramanian, and B. U. Nair, *Biochim. Biophys. Acta - Gen. Subj.*, 2000, **1475**, 157–162.
7. C. Ramakrishnan, V. Subramanian, K. Balamurugan, and D. Velmurugan, *J. Biomol. Struct. Dyn.*, 2012, **31**, 1277–1292.
8. J. Neugebauer and T. Hickel, *Wiley Interdiscip. Rev. Comput. Mol. Sci.*, 2013, **3**, 438–448.
9. J. Hafner and C. Wolverton, *MRS Bull.*, 2006, **31**, 659–668.
10. A. E. Mattsson, P. A. Schultz, M. P. Desjarlais, T. R. Mattsson, and K. Leung, *Model. Simul. Mater. Sci. Eng.*, 2005, **13**, R1.
11. S. Manne and H. E. Gaub, *Science*, 1995, **270**, 1480–1482.
12. R. J. Davey, S. N. Black, L. A. Bromley, D. Cottier, B. Dobbs, and J. E. Rout, *Nature*, 1991, **353**, 549–550.
13. N. L. Abbott, *AIChE J.*, 2001, **47**, 2634–2639.
14. B. Bag, B. Das, and B. K. Mishra, *Miner. Metall. Process.*, 2010, **26**, 226–232.
15. R. M. Cornell and U. Schwertmann, *The Iron Oxides: Structure, Properties, Reactions, Occurrences and Uses*, wiley-vch verlag gmbh & co. kгаа weinheim , NY, 2nd edn., 2006.

16. A. Pindred and J. A. Meech, *Int. J. Miner. Process.*, 1984, **12**, 193–212.
17. V. Jain, B. Rai, U. V. Waghmare, V. Tammishetti, and Pradip, *Trans. Indian Inst. Met.*, 2013, **66**, 447–456.
18. P. I. Pankratov and L. P. Skorodumova, *Sov. Min.*, 1970, **6**, 210–213.
19. S. M. Zhao, D. Z. Wang, Y. H. Hu, S. X. Bao, and J. Xu, *Miner. Eng.*, 2003, **16**, 1031–1033.
20. L. Xia, H. Zhong, and G. Liu, *Trans. Nonferrous Met. Soc. China*, 2010, **20**, 495–501.
21. W. Yuhua and R. Jianwei, *Int. J. Miner. Process.*, 2005, **77**, 116–122.
22. F. Guan, H. Zhong, G. Liu, S. Zhao, and L. Xia, *Trans. Nonferrous Met. Soc. China*, 2009, **19**, 228–234.
23. M. J. Frisch, G. W. Trucks, H. B. Schlegel, G. E. Scuseria, M. A. Robb, J. R. Cheeseman, G. Scalmani, V. Barone, B. Mennucci, G. A. Petersson, H. Nakatsuji, M. Caricato, X. Li, H. P. Hratchian, A. F. Izmaylov, J. Bloino, G. Zheng, J. L. Sonnenberg, M. Hada, M. Ehara, K. Toyota, R. Fukuda, J. Hasegawa, M. Ishida, T. Nakajima, Y. Honda, O. Kitao, H. Nakai, T. Vreven, J. Montgomery, J. E. Peralta, F. Ogliaro, M. Bearpark, J. J. Heyd, E. Brothers, K. N. Kudin, V. N. Staroverov, R. Kobayashi, J. Normand, K. Raghavachari, A. Rendell, J. C. Burant, S. S. Iyengar, J. Tomasi, M. Cossi, N. Rega, N. J. Millam, M. Klene, J. E. Knox, J. B. Cross, V. Bakken, C. Adamo, J. Jaramillo, R. Gomperts, R. E. Stratmann, O. Yazyev, A. J. Austin, R. Cammi, C. Pomelli, J. W. Ochterski, R. L. Martin, K. Morokuma, V. G. Zakrzewski, G. A. Voth, P. Salvador, J. J. Dannenberg, S. Dapprich, A. D. Daniels, O. Farkas, J. B. Foresman, J. V. Ortiz, J. Cioslowski and D. J. Fox, Gaussian 09, Revision B.01, Gaussian, Inc., Wallingford CT, 2009
24. S. F. Boys and F. Bernardi, *Mol. Phys.*, 1970, **19**, 553–566.

25. F. Biegler-Konieg, J. Schonbohm and D. Bayles, *J. Comput. Chem.*, 2001, **22**, 545–559.
26. B. Mennucci, J. Tomasi, R. Cammi, J. R. Cheeseman, M. J. Frisch, F. J. Devlin, S. Gabriel, and P. J. Stephens, *J. Phys. Chem. A*, 2002, **106**, 6102–6113.
27. A. Kremleva, S. Krüger, and N. Rösch, *Langmuir*, 2008, **24**, 9515–9524.
28. A. Kremleva, S. Krugera, and N. Rosch, *Phys. Chem. Chem. Phys.*, 2015, **17**, 13757–13768
29. I. Rozas and P. E. Kruger, *J. Chem. Theory Comput.*, 2005, **1**, 1055–1062.
30. H. Hong, X. Min, and Y. Zhou, *J. Wuhan Univ. Technol. Sci. Ed.*, 2007, **22**, 661–666.
31. C. E. White, J. L. Provis, D. P. Riley, G. J. Kearley, and J. S. J. Van Deventer, *J. Phys. Chem. B*, 2009, **113**, 6756–6765.
32. A. M. Scott, E. a Burns, and F. C. Hill, *J. Mol. Model.*, 2014, **20**, 2373.
33. M. M. Dawley, A. M. Scott, F. C. Hill, J. Leszczynski, and T. M. Orlando, *J. Phys. Chem. C*, 2012, **116**, 23981–23991
34. J. Farrell and B. K. Chaudhary, *Environ. Sci. Technol.*, 2013, **47**, 8342–8347
35. H. Yuehua, S. Wei, L. Haipu, and Z. Xu, *Miner. Eng.*, 2004, **17**, 1017–1022.
36. H. Yuehua, S. Wei, J. Hao, J. D. Miller, and K. Fa, *Int. J. Miner. Process.*, 2005, **76**, 163–172.
37. D. L. Geatches, A. Jacquet, S. J. Clark, and H. C. Greenwell, *J. Phys. Chem. C*, 2012, **116**, 22365–22374.
38. C. Appel, L. Q. Ma, R. D. Rhue, and E. Kennelley, *Geoderma*, 2003, **113**, 77–93.
39. B. K. Schroth and G. Sposito, *Clays Clay Miner.*, 1997, **45**, 85–91.
40. M. Tschapek, L. Tcheichvili, and C. Wasowski, *Clay Miner.*, 1974, **10**, 219–229.
41. X. Liu-yin, Z. Hong, L. Guang-yi, and L. Xin-gang, *J. Cent. South Univ. Technol.*, 2009, **16**, 73–79.
42. Z. Zhou and W. D. Gunter, *Clays Clay Miner.*, 1992, **40**, 365–368.

43. G. Feng, Z. Hong, L. Guan, Z. Sheng, X. L. Yin *Trans. Nonferrous Met. Soc. China* 2009, **19**, 228-234

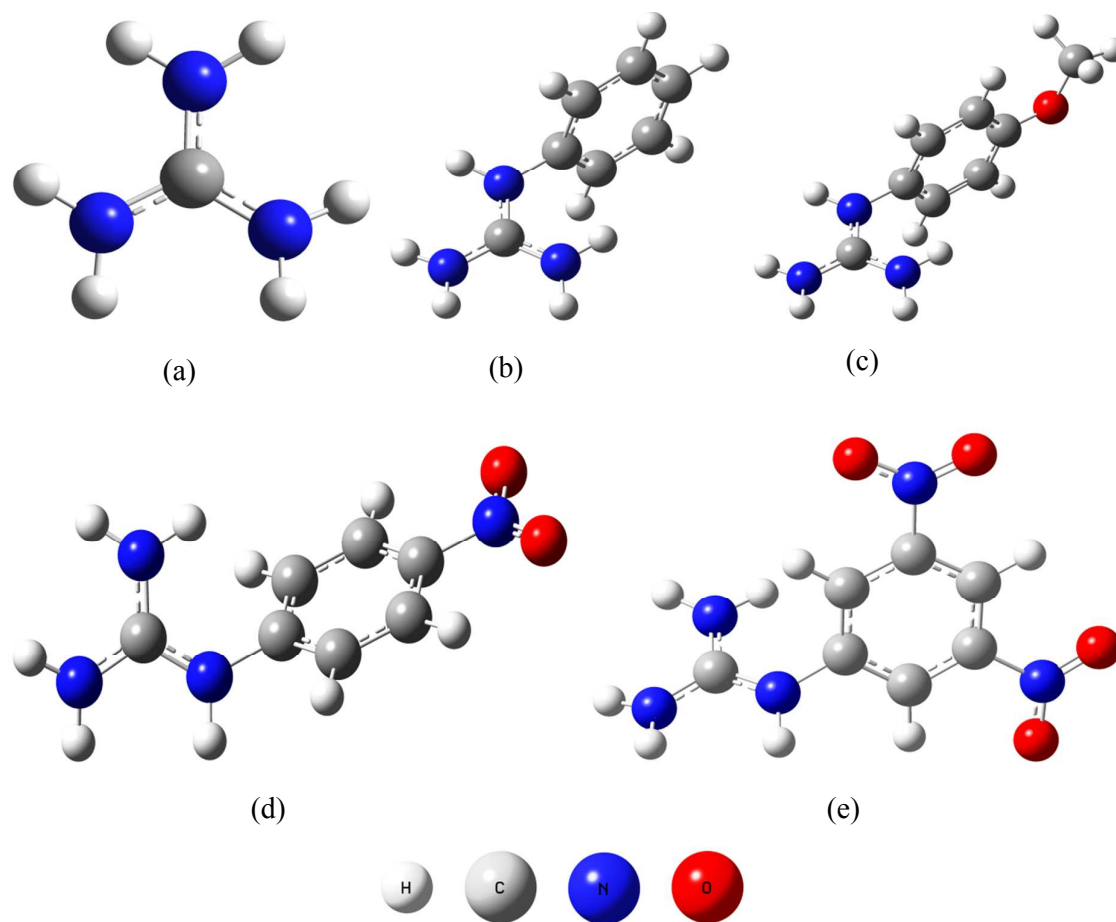


Fig. 1 The optimized geometries of five different guanidinium based cationic collectors. (a) Guanidinium cation (GC) (b) phenyl guanidinium cation (PGC) (c) methoxy phenyl guanidinium cation (MPGC) (d) p-nitro phenyl guanidinium cation (NPGC) and (e) 3,5 dinitro phenyl guanidinium cation (DNPGC).

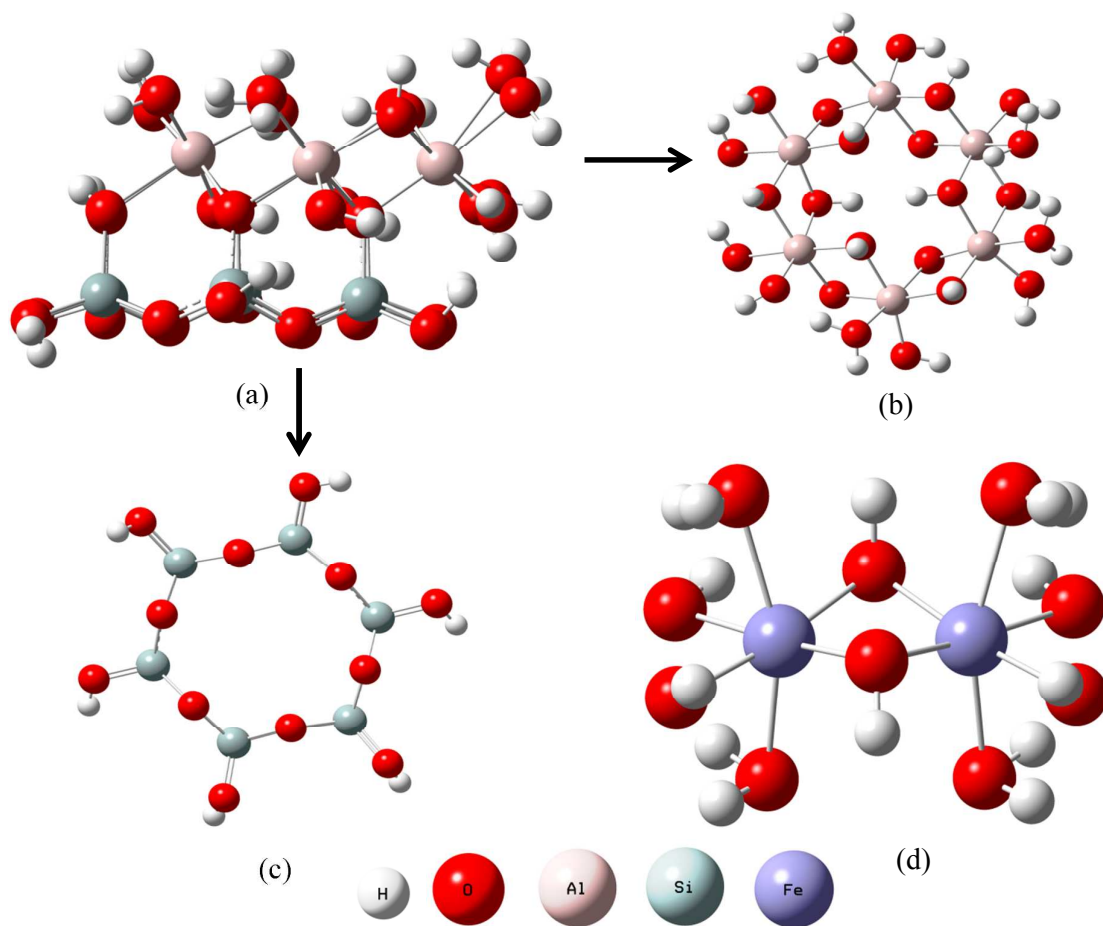


Fig. 2 The optimized geometries of kaolinite and goethite clusters. (a) Side view of the Kaolinite cluster (b) Top view of the K(a) surface (c) Top view of the K(s) surface and (d) goethite cluster.

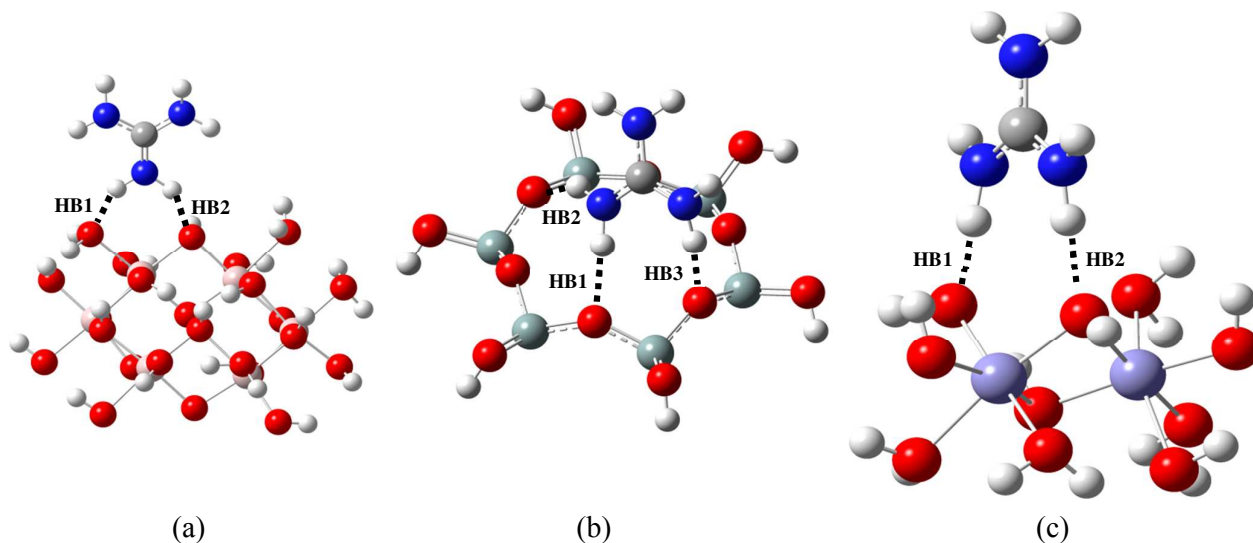


Fig. 3 The optimized geometries of GC on (a) K(a) surface, (b) K(s) surface and (c) goethite cluster in gas phase (The images were depicted with only half cluster of kaolinite for clarity).

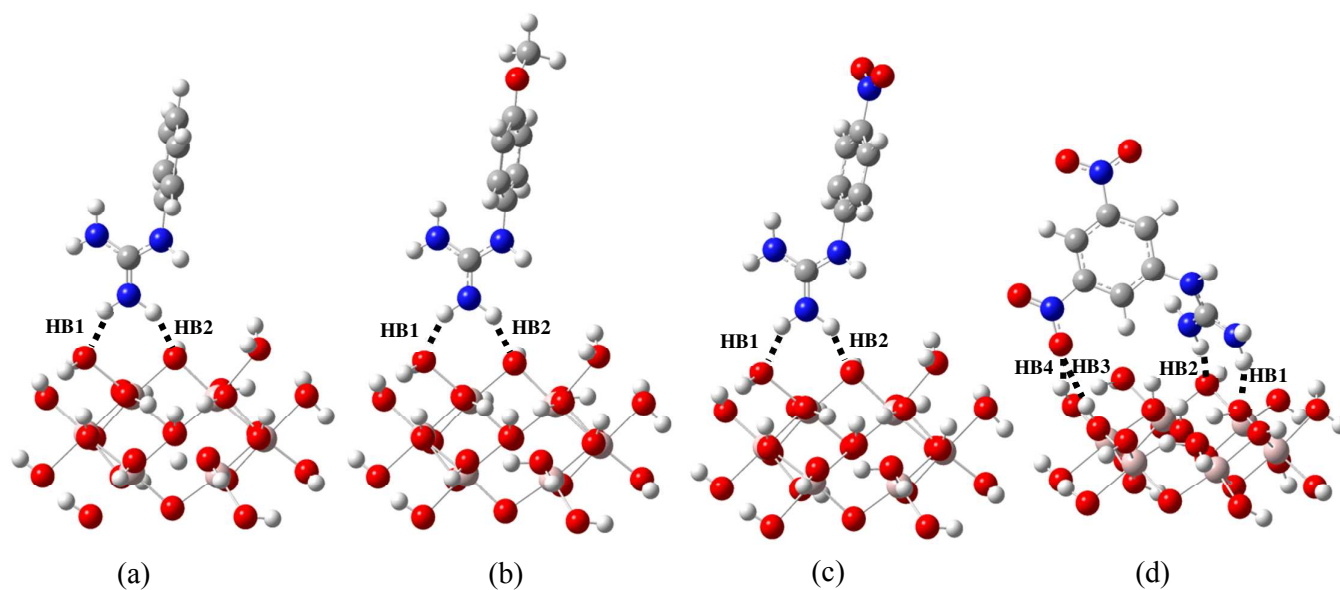


Fig. 4 The optimized geometries of various cationic collectors (a) PGC (b) MPGC (c) NPGC (d) DNPGC on K(a) surface in gas phase (The images were depicted with only half cluster of kaolinite for clarity).

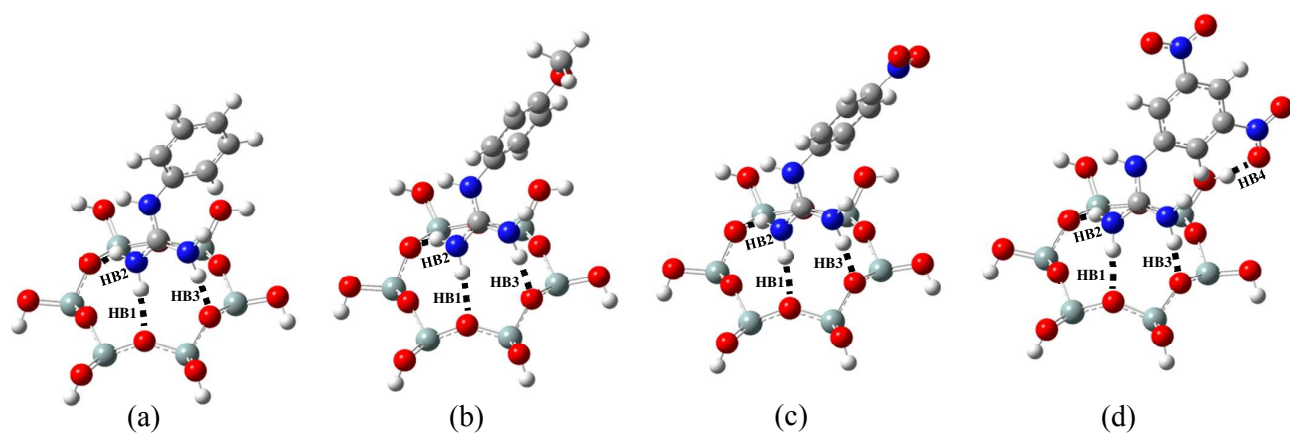


Fig. 5 The optimized geometries of various cationic collectors (a) PGC (b) MPGC (c) NPGC (d) DNPGC on K(s) surface in gas phase (The images were depicted with only half cluster of kaolinite for clarity).

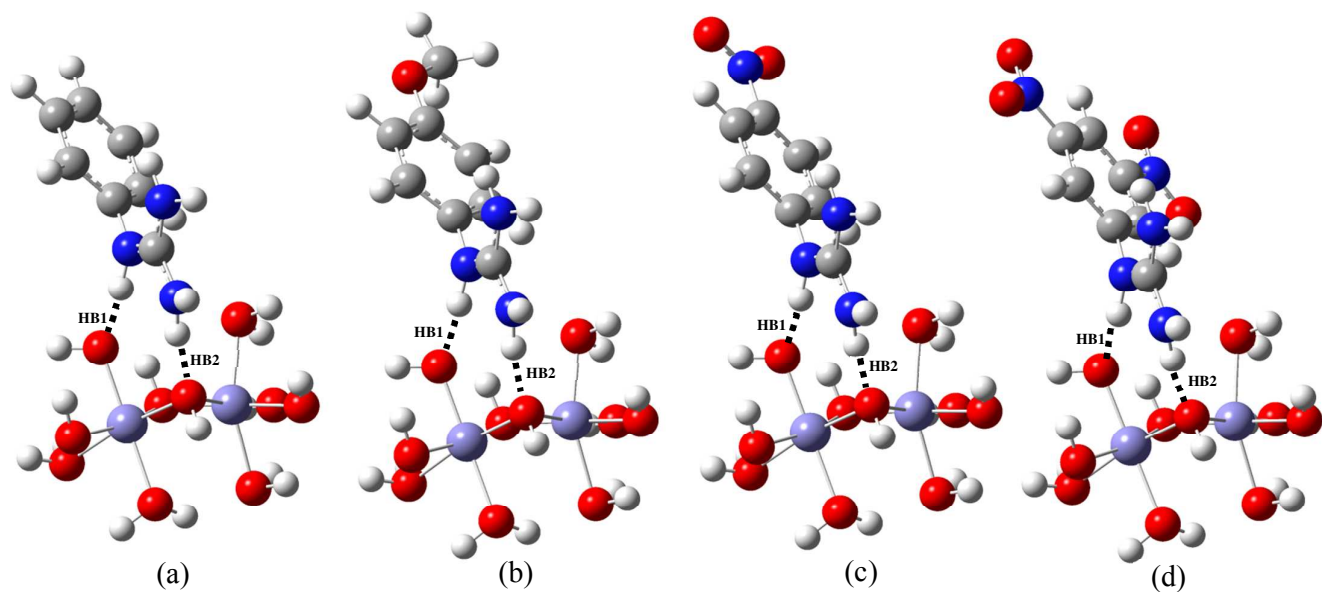


Fig. 6 The optimized geometries of various cationic collectors (a) PGC (b) MPGC (c) NPGC (d) DNPGC on goethite cluster in gas phase.

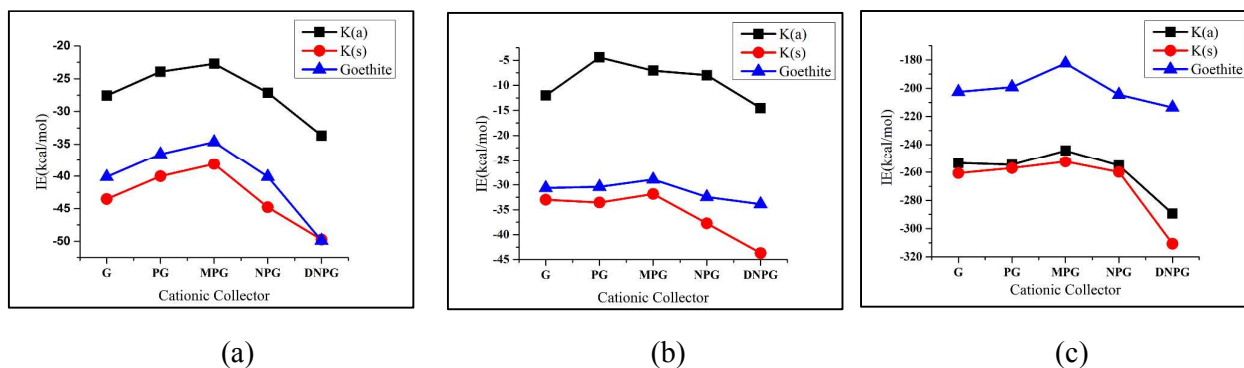


Fig. 7 The adsorption energies of five different guanidinium based cationic collectors on K (a), K(s) and goethite in (a) gas phase (b) explicit water model and (c) pH model (black, red and blue lines indicates interaction energy on K(a), K(s) and goethite surface, respectively).

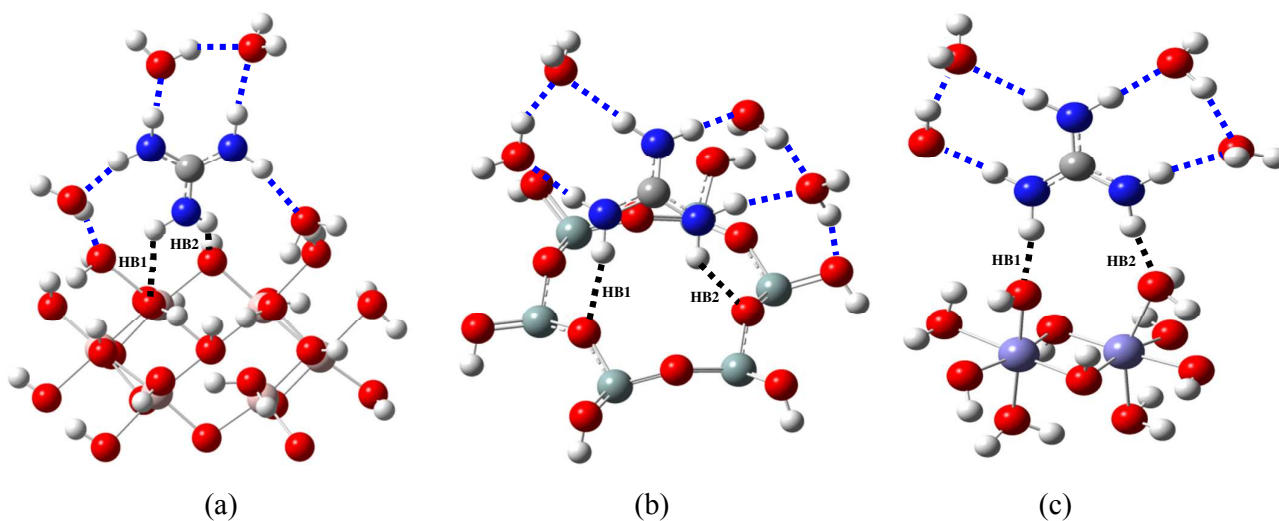


Fig. 8 The optimized geometries of GC on (a) K(a) surface, (b) K(s) surface and (c) goethite cluster in explicit water model. The blacked dashed lines represents the hydrogen bonds of collector with mineral surface and the blue dotted lines represents the inter hydrogen bonds between the water molecules as well as between the collector explicit water molecule. (The images were depicted with only half cluster of kaolinite for clarity).

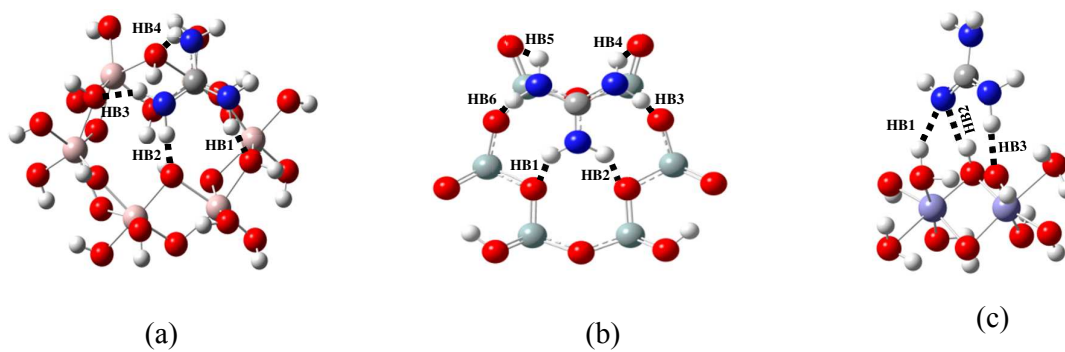


Fig. 9 The optimized geometries of GC on (a) K(a) surface, (b) K(s) surface and (c) goethite cluster in pH model.

Table 1. Calculated adsorption energies of various guanidinium based cationic collectors on K(a), K(s) and goethite clusters in gas, explicit water, implicit on explicit water and pH models (all the values are in kcal/mol).

Cation	Gas phase model								
	K(a)			K(s)			Goethite		
	6-31G(d)	6-31G(d,p)	6-31+G(d,p)	6-31G(d)	6-31G(d,p)	6-31+G(d,p)	6-31G(d)	6-31G(d,p)	6-31+G(d,p)
G	-27.57	-27.30	-25.04	-43.51	-43.59	-39.78	-40.10	-39.99	-36.64
PG	-23.94	-23.68	-21.46	-39.99	-40.06	-36.29	-36.53	-36.38	-33.07
MPG	-22.71	-22.46	-20.36	-38.12	-38.20	-34.49	-34.66	-34.58	-31.38
NPG	-27.13	-26.85	-24.50	-44.77	-44.84	-40.92	-40.08	-40.25	-36.87
DNPG	-33.67	-33.39	-31.27	-49.73	-49.87	-45.48	-49.90	-49.90	-46.45
Explicit Water model									
G	-12.02	-11.85	-8.12	-32.98	-32.80	-27.87	-30.63	-30.91	-26.51
PG	-4.43	-3.83	-1.19	-33.54	-33.36	-27.71	-30.38	-30.15	-26.36
MPG	-7.06	-6.91	-3.19	-31.83	-31.70	-25.43	-28.92	-28.85	-24.73
NPG	-7.96	-7.74	-4.14	-37.73	-37.58	-32.13	-32.44	-32.69	-28.26
DNPG	-14.50	-14.27	-10.65	-43.66	-43.69	-37.05	-33.88	-34.06	-29.84
Implicit + Explicit Water model									
G				-22.24	-21.83	-17.31	-18.27	-17.18	-13.52
PG				-20.55	-20.39	-15.75	-17.26	-16.20	-11.49
MPG				-20.60	-20.50	-14.68	-16.74	-15.67	-11.85
NPG				-26.97	-26.55	-22.11	-20.40	-19.12	-15.43
DNPG	-10.53	-10.55	-7.53	-32.45	-32.33	-25.38	-21.81	-20.61	-17.18
pH model									
G	-253.48	-252.86	-240.48	-260.68	-261.40	-249.44	-202.59	-203.17	-194.44
PG	-254.57	-254.26	-243.76	-257.01	-256.21	-247.21	-199.20	-199.95	-191.53
MPG	-244.24	-244.29	-234.17	-252.40	-251.74	-242.74	-182.43	-182.69	-175.78
NPG	-255.24	-254.06	-244.25	-259.80	-260.69	-250.12	-204.54	-206.29	-199.50
DNPG	-289.41	-288.16	-278.99	-310.71	-309.83	-302.07	-213.60	-215.25	-208.31

Table 2. Calculated hydrogen bond parameters (bond length (BL), bond angle (BA) total electron density $\rho(r_c)$, laplacian of electron density ($\nabla^2\rho(r_c)$) at the bond critical points) of various guanidinium based cationic collectors on K(a), K(s) and goethite clusters in gas phase model (the bond lengths are in Å , the bond angles are in degrees and electron densities are in a.u).

Cation	HB1				HB2				HB3				HB4			
	BL	BA	$\rho(r_c)$	$\nabla^2\rho(r_c)$												
K (a)																
GC	1.92	142.33	0.0402	0.0315	1.77	151.38	0.0302	0.0224								
PGC	1.91	144.44	0.0355	0.0277	1.83	146.91	0.0305	0.0226								
MPGC	1.94	143.58	0.0354	0.0275	1.83	147.96	0.0290	0.0216								
NPGC	1.89	144.75	0.0378	0.0295	1.80	148.32	0.0325	0.0241								
DNPGC	1.77	156.71	0.0418	0.0307	1.73	166.91	0.0451	0.0328	2.39	137.56	0.0079	0.0087	2.20	153.30	0.0200	0.0174
K (s)																
GC	1.93	173.85	0.0280	0.0210	2.43	146.46	0.0096	0.0088	1.93	159.14	0.0280	0.0210				
PGC	1.95	173.69	0.0266	0.0198	2.49	145.21	0.0084	0.0080	1.94	159.67	0.0277	0.0209				
MPGC	1.97	169.87	0.0257	0.0191	2.43	148.67	0.0095	0.0087	1.99	156.48	0.0250	0.0189				
NPGC	1.94	172.76	0.0274	0.0203	2.41	148.36	0.0099	0.0089	1.91	158.66	0.0291	0.0220				
DNPGC	1.95	167.37	0.0266	0.0196	2.29	153.75	0.0130	0.0107	1.89	155.16	0.0308	0.0235	2.02	152.71	0.0199	0.0174
Goethite																
GC	1.61	176.43	0.05878	0.0420	1.71	176.07	0.0385	0.0286								
PGC	1.64	174.88	0.05553	0.0405	1.82	171.91	0.0362	0.0270								
MPGC	1.65	175.57	0.05355	0.0395	1.83	171.09	0.0351	0.0262								
NPGC	1.61	174.26	0.05983	0.0428	1.81	172.93	0.0372	0.0277								
DNPGC	1.58	173.96	0.06444	0.0449	1.81	173.60	0.0374	0.0277								

Table 3. Calculated hydrogen bond parameters (bond length (BL), bond angle (BA) and total electron density $\rho(r_c)$, laplacian of electron density ($\nabla^2\rho(r_c)$) at the bond critical points) of various guanidinium based cationic collectors on K(a), K(s) and goethite clusters in explicit water model (the bond lengths are in Å , the bond angles are in degrees and electron densities are in a.u).

Cation	HB1				HB2				HB3				HB4			
	BL	BA	$\rho(r_c)$	$\nabla^2\rho(r_c)$												
K (a)																
GC	2.18	121.20	0.0183	0.0155	1.98	147.16	0.0265	0.0200								
PGC	1.99	158.53	0.0260	0.0189												
MPGC	1.99	159.36	0.0260	0.0188												
NPGC	1.91	168.74	0.0300	0.0220												
DNPGC	1.92	146.04	0.0306	0.0234	1.91	164.11	0.0304	0.0217	2.23	138.66	0.0124	0.0119	2.04	156.57	0.0194	0.0170
K (s)																
GC	2.39	152.23	0.0101	0.0090	2.16	135.55	0.0173	0.0144								
PGC	2.05	140.09	0.0218	0.0179	2.04	169.54	0.0220	0.0168								
MPGC	2.04	140.75	0.0220	0.0168	2.04	168.96	0.0221	0.0181								
NPGC	2.09	162.47	0.0199	0.0153	2.13	170.87	0.0181	0.0139								
DNPGC	1.94	160.43	0.0273	0.0206	2.31	158.10	0.0123	0.0105	2.04	149.98	0.0222	0.01771	2.08	149.54	0.0176	0.0152
Goethite																
GC	1.77	172.01	0.0399	0.0304	1.96	166.35	0.0260	0.0198								
PGC	1.66	169.82	0.0546	0.0384	1.87	174.18	0.0322	0.0241								
MPGC	1.67	169.42	0.0527	0.0371	1.80	165.90	0.0376	0.0291								
NPGC	1.60	172.59	0.0610	0.0426	1.79	162.45	0.0386	0.0295								
DNPGC	1.73	170.56	0.0454	0.0324	1.78	160.59	0.0392	0.0313								

Table 4. Calculated hydrogen bond parameters (bond length (BL), bond angle (BA) and total electron density $\rho(r_c)$, laplacian of electron density ($\nabla^2\rho(r_c)$) at the bond critical points) of various guanidinium based cationic collectors on K(a), K(s) and goethite cluster in pH model (the bond lengths are in Å , the bond angles are in degrees and electron densities are in a.u).

Cation	HB1				HB2				HB3				HB4				HB5				HB6										
	BL	BA	$\rho(r_c)$	$\nabla^2\rho(r_c)$	BL	BA	$\rho(r_c)$	$\nabla^2\rho(r_c)$	BL	BA	$\rho(r_c)$	$\nabla^2\rho(r_c)$	BL	BA	$\rho(r_c)$	$\nabla^2\rho(r_c)$	BL	BA	$\rho(r_c)$	$\nabla^2\rho(r_c)$	BL	BA	$\rho(r_c)$	$\nabla^2\rho(r_c)$	BL	BA	$\rho(r_c)$	$\nabla^2\rho(r_c)$			
K (a)																															
GC	1.91	142.66	0.0314	0.0230	1.60	162.54	0.0609	0.0435	2.67	133.65	0.0068	0.0065	2.0910	145.77	0.0214	0.0162															
PGC	2.01	146.76	0.0252	0.0180	1.68	159.40	0.0507	0.0386	1.96	156.85	0.0278	0.0201	1.8050	161.35	0.0396	0.0269															
MPGC	1.97	133.96	0.0290	0.0206	1.67	154.61	0.0524	0.0398	1.62	160.23	0.0580	0.0405																			
NPGC	1.88	175.96	0.0427	0.0298	1.70	156.21	0.0621	0.0402	2.36	141.13	0.0173	0.0125	2.2452	134.65	0.0198	0.0154															
DNPGC	1.72	176.81	0.0464	0.0327	1.56	157.82	0.0666	0.0455	2.15	143.13	0.0198	0.0141	2.1124	136.86	0.0207	0.0166															
K (s)																															
GC	2.16	139.18	0.0180	0.0140	2.14	144.76	0.0183	0.0143	2.32	122.24	0.0140	0.0130	1.98	142.39	0.0292	0.0134	2.49	122.87	0.0117	0.0100	2.14	137.87	0.0193	0.0155							
PGC	2.67	137.31	0.0069	0.0067	1.93	158.85	0.0289	0.0210	2.20	144.15	0.0167	0.0126	2.05	130.60	0.0235	0.0183	1.98	155.54	0.0293	0.0187											
MPGC	2.08	135.73	0.0210	0.0177	2.06	126.41	0.0219	0.0187	2.07	147.95	0.0221	0.0163	2.05	139.19	0.0235	0.0175															
NPGC	2.36	136.72	0.0128	0.0101	2.50	137.83	0.0089	0.0087	1.80	173.76	0.0366	0.0282	2.03	130.06	0.0242	0.0185															
DNPGC	1.75	175.19	0.0077	0.0076	2.37	119.01	0.0131	0.0118	1.77	148.86	0.0433	0.0309																			
GOETHITE																															
GC	1.96	152.29	0.0300	0.0209	2.08	167.43	0.0236	0.0163	1.78	171.40	0.0413	0.0297																			
PGC	1.89	165.73	0.0350	0.0233	1.85	165.57	0.0350	0.0253																							
MPGC	2.02	145.60	0.0489	0.0356	1.70	176.52	0.0267	0.0186																							
NPGC	1.84	173.47	0.0404	0.0251	1.67	168.98	0.0578	0.0341	1.90	158.03	0.0350	0.0225																			
DNPGC	1.82	158.25	0.0409	0.0265	2.00	168.23	0.0287	0.0191	1.84	168.84	0.0402	0.0255	1.92	168.26	0.0335	0.0216															